Electronic Materials Letters (2023) 19:38–54
https://doi.org/10.1007/s13391-022-00378-0

ORIGINAL ARTICLE - ENERGY AND SUSTAINABILITY

Toward High-Performance Quinoxaline Based Non-fullerene Small Molecule Acceptors for Organic Solar Cells

Amna Ayub[1] · Muhammad Ans[1] · Sehrish Gul[1] · Ahmed M. Shawky[2] · Khurshid Ayub[3] · Javed Iqbal[1,6] · Muhammad Ali Hashmi[4] · Ahmed Lakhani[5]

Received: 9 August 2022 / Accepted: 27 September 2022 / Published online: 28 October 2022
© The Author(s) under exclusive licence to The Korean Institute of Metals and Materials 2022

Abstract

Unfused non-fullerene acceptors with the advantages of simple synthesis, high yields, and low cost have received a lot of interest in recent years. Herein, we designed five structures (UF-M1–UF-M5) with unfused non-fullerene acceptors coupled to electron-deficient quinoxaline (Qx) as the core unit via electron-donating cyclo-penta-dithiophene (CPDT) as the conjugated backbone by modification in UF-Qx-2Cl taken as reference. Among all, mPW1PW91 method predicted λ_{max} closest to the λ_{max} of UF-Qx-2Cl, so we implemented the mPW1PW91 method with a 6-31G(d,p) basis set for the optimization of designed geometries and their molecular electrostatic mapping (MEP). Further parameters like FMOs (frontier molecular orbitals), TDM (transition density matrix analysis), DOS (density of state analysis), electron–hole mobility rate (reorganization energies), dipole moment, and chemical quantum descriptive parameters were evaluated for organic photovoltaics. Among all, UF-M4 predicted better absorption in the gaseous and solvent phase (λ_{max} = 726 nm and 789 nm respectively), lower bandgap (E_g = 2.03 eV), higher dipole moment (1.99 and 5.33 debye in gaseous and solvent phase respectively), better quantum chemical descriptive parameters, and higher electron mobility rate (λ_e = 0.00766 eV). The results reveal that the acceptor molecule UF-M4 that has been created performs better in studies and better opportunities for organic-photovoltaics. To summarize, the unfused non-fullerene-based acceptor modification technique has shown effective in paving the way for the development of promising photovoltaic materials. All currently projected acceptor contributors (UF-M1–UF-M5) should be targeted to produce future competent organic photovoltaics.

✉ Muhammad Ans
ansbhatti24@gmail.com

✉ Khurshid Ayub
khurshid@cuiatd.edu.pk

✉ Javed Iqbal
Javed.Iqbal@uaf.edu.pk; Javedkhattak79@gmail.com; Jiqbal@uob.edu.bh

[1] Department of Chemistry, University of Agriculture, Faisalabad 38000, Pakistan

[2] Science and Technology Unit (STU), Umm Al-Qura University, Makkah 21955, Saudi Arabia

[3] Department of Chemistry, COMSATS University Islamabad, Abbottabad Campus, Abbottabad 22060, KPK, Pakistan

[4] Department of Chemistry, Division of Science & Technology, University of Education, Lahore 54770, Pakistan

[5] Department of Biomedical and Health Sciences, Calumet College of St. Joseph, 2400, New Your Ave, Whiting, IN 4639, USA

[6] Department of Chemistry, College of Science, University of Bahrain, P.O. Box 32038, Zallaq, Bahrain

Graphical Abstract

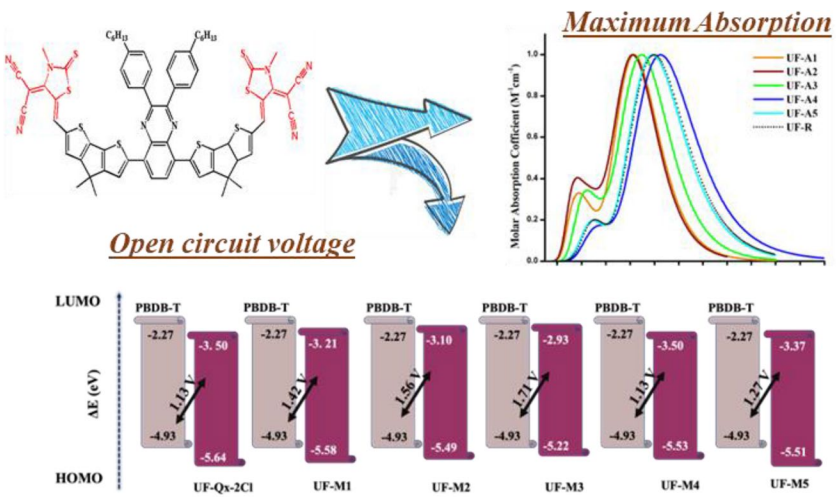

Keywords Organic solar cells · Density functional theory · Opto-electronic properties · Energy gap

1 Introduction

For decades, there has been a serious problem with the energy crisis and the desire for environmentally friendly energy sources [1]. Fossil fuels and other non-renewable energy sources are declining day by day and also emit hazardous gases, CO_2 harms the environment [2]. Many new power generation technologies are emerging recently, including hydropower plants, wind power, solar cells, and biomass [3, 4]. Although nuclear power is a powerful source of energy, it is considered a non-environmentally friendly and unreliable source of energy due to the recent catastrophe in Japan, radioactive wastes, and security thread [1]. In all of these situations, the solar cell is considered a reliable, environmentally friendly, and energy-efficient source for managing energy disasters [5]. Converting sunlight into electricity in photovoltaic cells (PVCs) is a good alternative to generating electricity to meet world demand [6]. Various PVCs have been introduced in the market since the nineteenth century, including crystalline-silicon based, thin films, dye-sensitized, semiconductor-based and organic material based, and all these materials are beneficial enough to meet the energy demands. Although inorganic solar cell like silicon-based is abundant, nontoxic, and thermally stable along with high energy production they have some flaws too i.e., having high fabrication cost, rigid structure along with low efficiency because of their non-tunable energy levels [7].

Among all, organic solar cells are considered an emerging energy generating source with low cost, high efficiency, flexibility, processability at low temperature, and easy fabrication process [8, 9]. Organic photovoltaics are composed of two basic constituents, named p-type and n-type semiconductors. N-type is referred to as an electron acceptor, whereas P-type is an electron donor. Organic solar cells can synthesize by three different strategies, first of them is to synthesize by p–n junction-based material, showing proficiency up to 15% [10, 11]. Second way is to use donor–acceptor type material with fused layer to enhance the proficiency of solar cell while third one is based on bulk heterojunction (BHJ), basically composed of conjugated polymer act as like electron-donating moiety with fullerene acceptor [12]. BHJ-based photovoltaic cells can easily fabricate by solution processing and have shown almost 15% more proficiency in comparison to conventional cells. In the last few years, BHJ photovoltaic showed approximately 11% increase in performance and proficiency but also experienced some limitations such as photochemical instability, aggregates formation, and a decrease in power conversion because of fullerene acceptor complexity, high bandgap and heat instability too [13, 14]. These facts are major hurdles in the commercial application of fullerene-based photovoltaic cells, so non-fullerene acceptors (NFA) are introduced in solar cells to overcome these limitations [15–17] as they exhibit narrow bandgap besides thermal, oxidative, and photochemical stability and show 6% increase in working efficiency [16]. NFAs have a strong absorption capacity and their peaks can be easily resolved, as well as a good ability to transport electrons [18]. Because of their simple structure, commercially they can easily fabricate. Non-fullerene acceptors revealed in literature are perylene diimides [19], benzo (1, 2-b: 4,5-b) di-thiophene (BDT) [20–22], TT [23–25], BZPT [11],

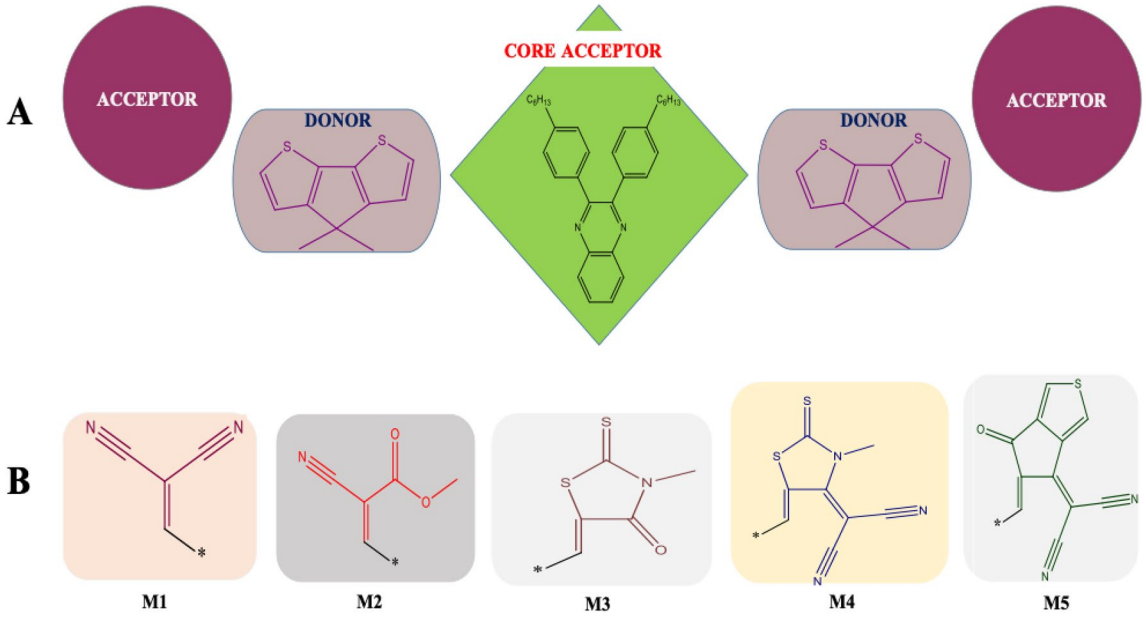

Scheme 1 **A** Core acceptor and donor of reference molecule based on A-D-A-D-A strategy **B** Structures of designed acceptor molecules

IDTT [26] and tetra-phenyl-ethylene which having planner fused ring structures with wide range absorption band and efficiently charge transfer. Although these fused ring NFAs enhance the proficiency of organic solar cells by up to 18%, the major issue is their synthesis, which is commercially too costly. To maneuver these issues, non-fused NFAs subunits with conformational lock give out a new approach to reduce the synthetic cost along with a simple synthetic route [27–36]. Non-fused NFAs use the single bond to make connections with adjacent subunits. To maintain a balance between HOMO & LUMO and bandgap, modifications are introduced by the usage of conjugated backbone, side-chain engineering, or end group replacement.

Here, we designed five molecules (UF-M1, UF-M2, UF-M3, UF-M4, UF-M5) by using non-fused acceptors on both edges of the reference molecule [37] utilizing A-D-A-D-A strategy. Reference molecule (UF-Qx-2Cl) has quinoxaline as a core which is electron-deficient and has wide use in conjugated A-D copolymers and helps to strengthen the resonance effect [38–40] while cyclo-Penta-di-thiophene (CPDT) is an electron-donating moiety, act as like spacer to enhance the absorption range with narrow bandgap as shown in Scheme 1.

This molecule is recently reported as a material with a higher PCE of 10.81%. We substituted five different acceptor subunits shown in Scheme 1 to reference molecule (UF-Qx-2Cl) to enhance the optoelectronic properties and broaden absorption range. We studied and compared the properties of designed molecules with reference molecules to study the effect of different acceptor substitutions and discussed the results in detail below, as molecular structures are represented in Fig. 1.

2 Methodology

All of the structures are designed on gauss view 5.0 [41] and all of the calculations are carried out through the gaussian 09 packages [42]. Firstly we optimized the reference molecule [37] by implementation of four functionals as B3LYP [43], CAM-B3LYP [44], mPW1PW91 [45], ωB97XD [46] along with basis set 6-31G(d,p) to optimized it to ground state and calculate its energy in a gaseous state and insolvent. We calculated the energy of the reference molecule [37] with different functions to make sure the selected functional provides λ_{max} nearest to experimental value. In our case, mPW1PW91/6-31G(d,p) bestowed the value 753 nm nearest to the experimental value of UF-Qx-2Cl i.e., 772 nm. So we selected mPW1PW91/6-31G(d,p) for further study.

We optimized our designed molecules (UF-M1–UF-M5) at mPW1PW91/6-31G(d,p) to make them geometrically stable. After optimization, TD-DFT is employed to analyze the excitation states of designed molecules in both phases i.e., gaseous and chloroform-solvent. Utilizing origin 6.0 professional software, obtained values of λ_{max} are plotted [47]. Transition-density matrix(TDM) and density of state (DOS) studies are also carried out at mPW1PW91/6-31G(d,p) level while software used for visualization of TDM is Multiwfn [48] and PyMOlyze1.1 software for DOS [49]. Reorganization energy is also delibrated via same functional as

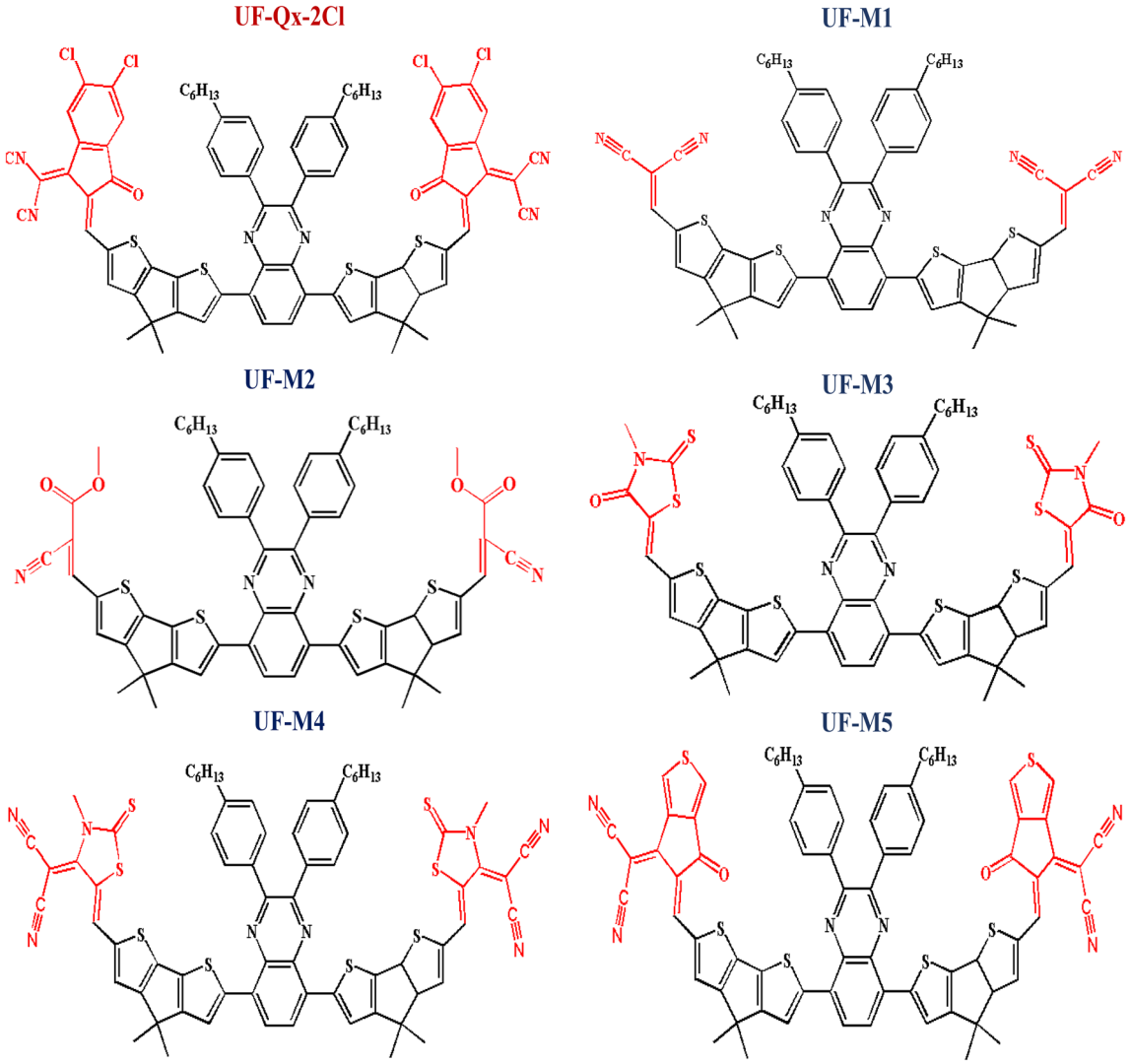

Fig. 1 Chemdraw sketch of reference and designed molecules

mPW1PW91/6-31G(d,p). All, designed and reference molecules are optimized at the cationic and anionic levels besides of neutral state.

$$\lambda = \lambda_i + \lambda_0 \tag{1}$$

The reorganization energy equation (Eq. 1) is used to modelize the electron–hole transfer rate, usually, two components of this energy are described i.e., internal (λ_i) and external reorganization energy (λ_0) [50]. External energy demonstrates the polarization effect when charge transfer occurs while internal energy explains the internal cationic and anionic geometrical changes of reference and design molecules. So we only focused on internal reorganization energy and electron–hole mobility is predicted by using the equations (Eqs. 2 and 3).

$$\lambda_- = \left[E_0^- - E_-\right] + \left[E_-^0 - E_0\right] \tag{2}$$

$$\lambda_+ = \left[E_0^+ - E_+\right] + \left[E_+^0 - E_0\right] \tag{3}$$

E_0^-, E_0^+ (Energy of anion and cation of neutrally optimized structure)

E_+^0, E_-^0 (Neutral energy of optimized cation and anion later normal optimization)

E_0 (Single point energy of simple optimized structure while E_+, E_- is the energy of cation and anion later optimization).

3 Results and Discussion

Calculated λ_{max} of reference (UF-Qx-2Cl) at different levels (B3LYP, CAM-B3LYP, mPW1PW91, and ωB97XD) are as follows 808.13 nm, 585.8 nm, 753.87 nm, 557.34 nm

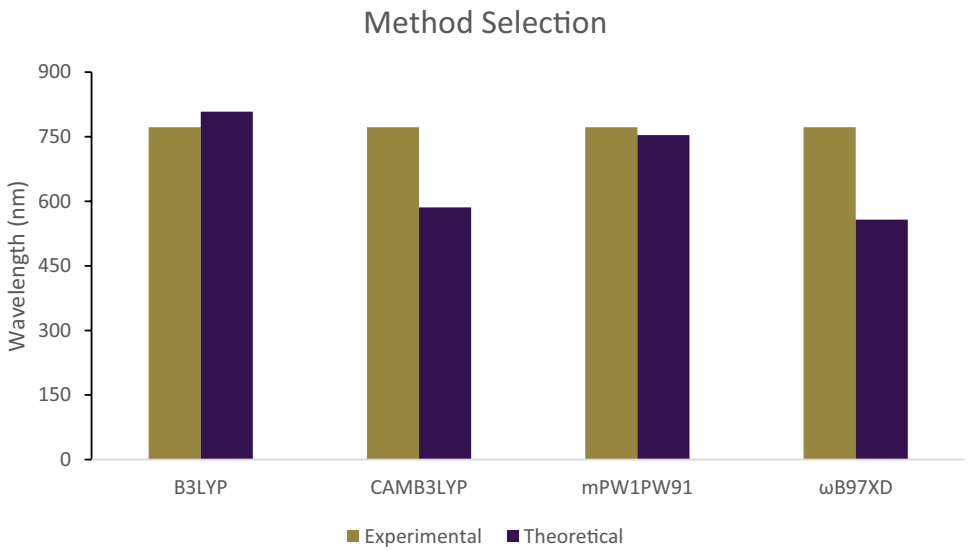

Fig. 2 Calculated λ_{max} value of reference molecule in solvent (chloroform) phase by different functionals

respectively while a reported experimental value of reference molecule in literature is 772 nm as represented in Fig. 2.

The mPW1PW91/6-31G(d,p) approach produced the results that come the closest to meeting the experimental value of UF-Qx-2Cl, so we selected mPW1PW91/6-31G(d,p) as a preferable approach for optimization and opto-electronic study of modified molecules. We optimized our modified molecules (UF-M1–UF-M5) with the selected method and the optimized structures are shown in Fig. 3.

The geometry of a molecule has an intense effect on its optical and electronic properties [51, 52]. Our reference molecule has a planer quinoxaline core acceptor with slightly curvy substituted groups. As we mentioned earlier that our reference molecule is based on the C-D-A strategy, so donor moieties on both sides of the acceptor core are substituted in a planer way along with the substitution of the alkyl group to show some steric effect to enhance the stability of the molecule. While acceptors of reference moiety are attached in some curvy manner and show dihedral angle which lowers the potential energy surface.

Table 1 carry the values for dihedral angle and bond length of acceptor moieties of UF-Qx-2Cl and designed molecules to their donors. Designed models show the dihedral angle above 130° results in a non-planar structure with a conformational lock which is sterically hindered and have a slighter possibility to show free rotation. Besides of dihedral angle, designed molecules also show a shorter bond length with a resonating effect that helps to strengthen the molecule stability.

3.1 Frontier-Molecular Orbitals (FMO) Analysis

In FMO analysis, HOMO as highest occupied MO's and LUMO as lowest occupied MO's are observed to calculate bandgap, an energy difference between conducting-valance orbital. The smaller distance between HOMO–LUMO makes it easier for an electron to shift from conducting orbital to valance orbital because of the smaller bandgap [53–55]. This concept can easily understand through the following formula, $\sigma \alpha \exp^{-Eg/KT}$ as K is Boltmanz constant, R is Temperature and E_g is bandgap while σ is electrical conductivity. This formula shows that electrical conductivity is directly related to bandgap and as we know that the smaller the value in exponential, the higher will be the outcome. FMOs analysis predicts the electric conductivity, Voc (open-circuit voltage), structural stability, charge generation, and PCE (power-conversion efficiency). FMO distribution and their graphical representation for reference and designed molecules (Figs. 4 and 5).

In reference molecule, HOMO has low charge density on acceptor while LUMO shows higher charge density on core acceptor and side substituted acceptors. Like reference molecules, our designed molecules (UF-M1–UF-M5) also showed better electron density on LUMO. Calculated values of HOMO, LUMO, bandgap, and binding energies in both phases i.e., gaseous and solvent along with interaction coefficient are depicted in Table 2.

Explored values trend of HOMO is as UF-M3 > UF-M2 > UF-M5 > UF-M4 > UF-M1 > UF-Qx-2Cl while trend in LUMO is as following UF-M3 > UF-M2 > UF-M1 > UF-M5 > UF-Qx-2Cl > UF-M4 shown in Fig. 5a. Equation 4 is used to compute the energy difference between HOMO–LUMO, which is the bandgap.

$$E_g = E_{LUMO} - E_{HOMO} \quad (4)$$

A smaller value of the bandgap indicates the strong pull of electrons by an electron acceptor. E_g value for

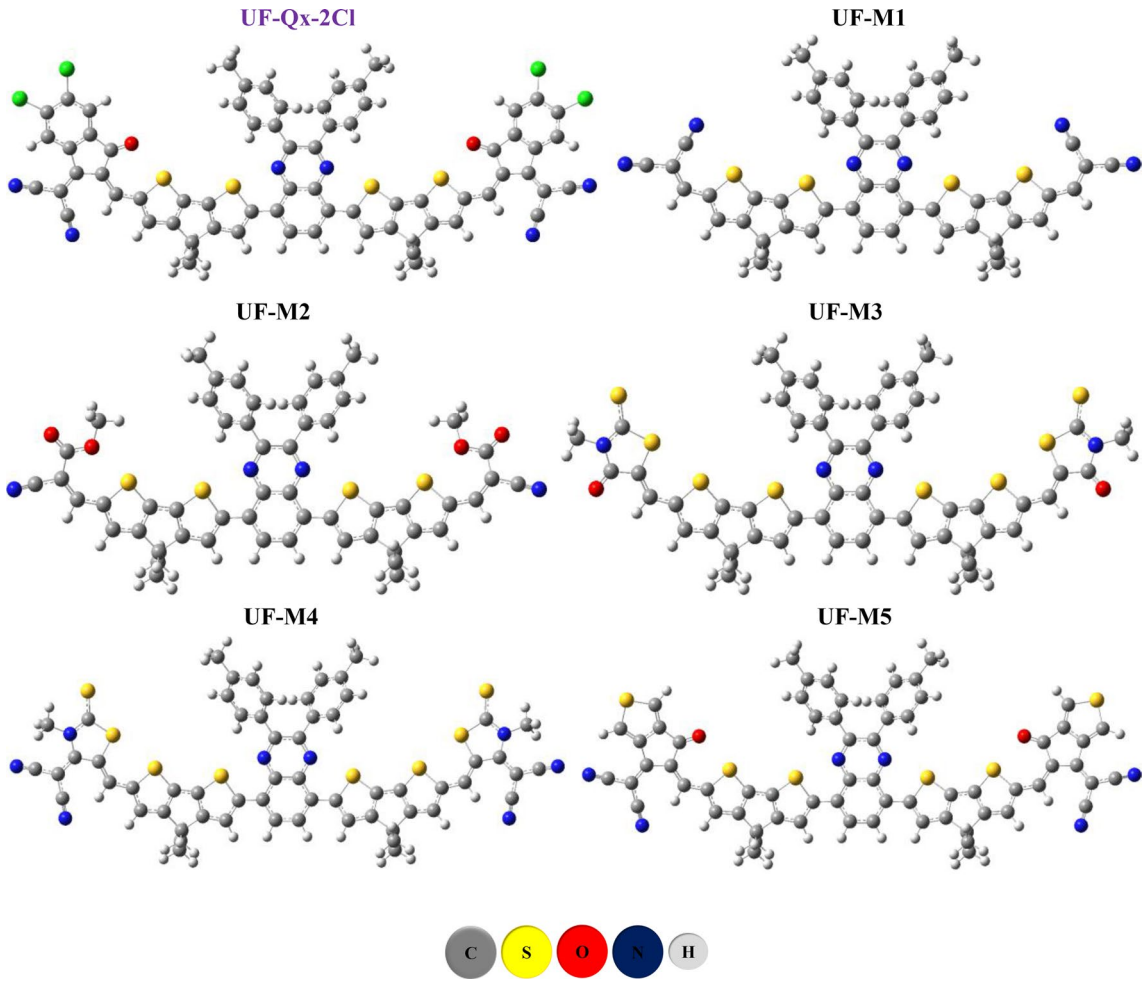

Fig. 3 Geometrically optimized structures of UF-Qx-2Cl and UF-M1–UF-M5

Table 1 Bond length (*Å*) and Dihedral angle (θ) of optimized moieties

Molecules	Dihedral angle (θ)	Bond length (*Å*)
UF-Qx-2Cl	134.14	1.38
UF-M1	130.79	1.37
UF-M2	137.58	1.37
UF-M3	131.08	1.35
UF-M4	130.98	1.37
UF-M5	134.35	1.38

all mioeties i.e.,reference and designed are as following UF-M4 (2.02) < UF-M5 ≈ UF-Qx-2Cl (2.14) < UF-M3 (2.29) < UF-M1 (2.36) < UF-M2 (2.41) represented in Fig. 5b. In our case, UF-M4 represents the smaller bandgap in relevancy to reference while UF-M5 shows almost the same bap gap as shown by reference. This lower band is due to a strong electron-withdrawing group along with a conjugated thiophene ring. In the UF-M4 molecule, CN a strong electron-withdrawing group is substituted on thiophene which resonates electron on whole acceptor subunit which reduces bandgap.

3.2 Molecular-Electrostatic-Potential Mapping

Molecular-electrostatic-potential mapping is a charge distribution visualization on structure and mobility of charge across donor to acceptor. By MEP mapping, we estimate the active sites of molecules as exposed for other molecules to attack. It's a colorful mapping in which the red color represents the negative charge density (electrophilic region) and the blue region shows positive charge density (nucleophilic region) while the green color is a representation of the neutral region shown in Fig. 6 along with their numerical values. In understudy molecules (UF-Qx-2Cl and UF-M1–UF-M5), the blue region is located on donor moiety which indicates the charge transfer across donor- acceptor while the red region is present on acceptor moieties but its density varies between designed molecules. Oxygen atoms in acceptor

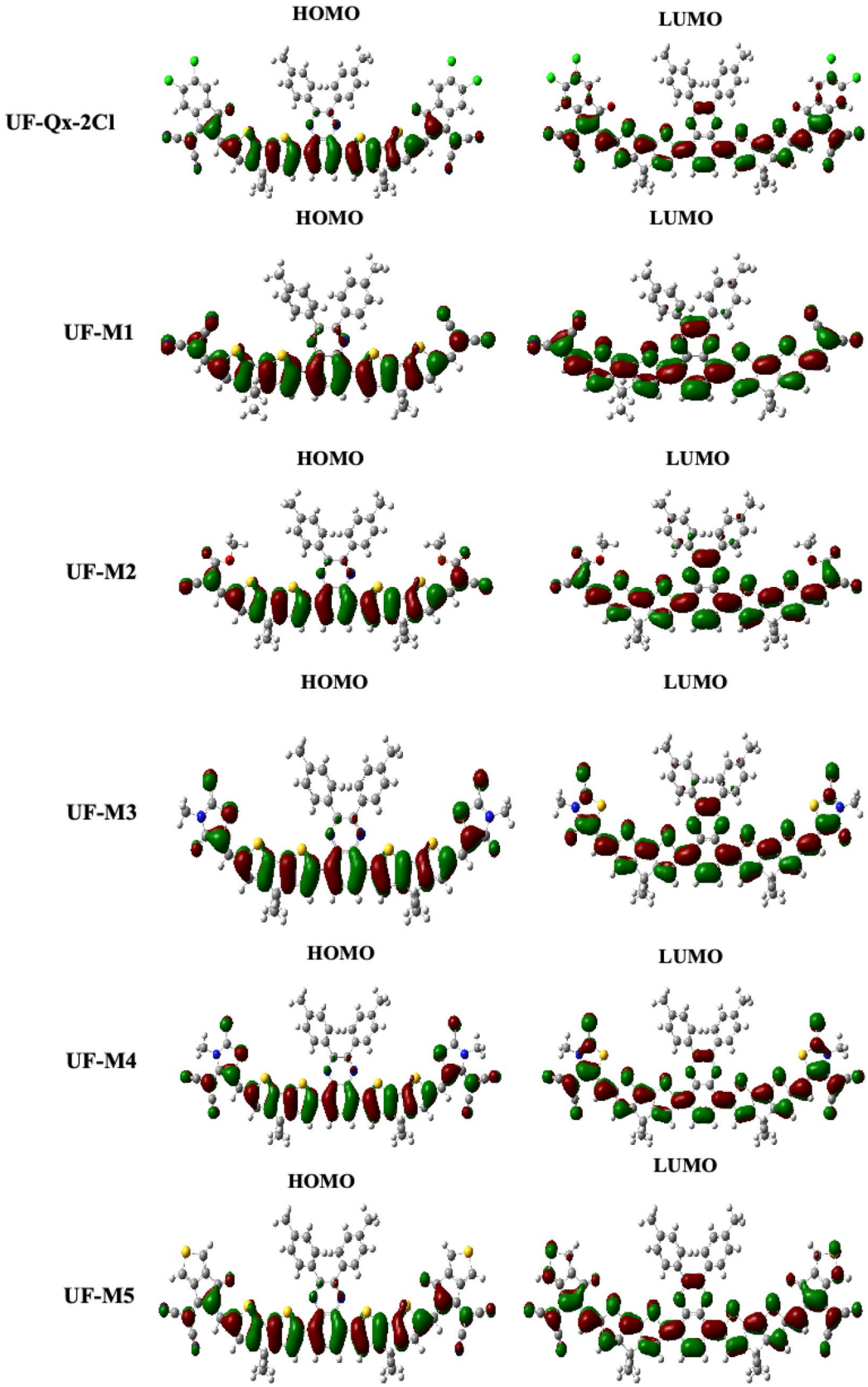

Fig. 4 Frontal-molecular-orbital's representation of reference asUF-Qx-2Cl and designed series of UF-M1–UF-M5

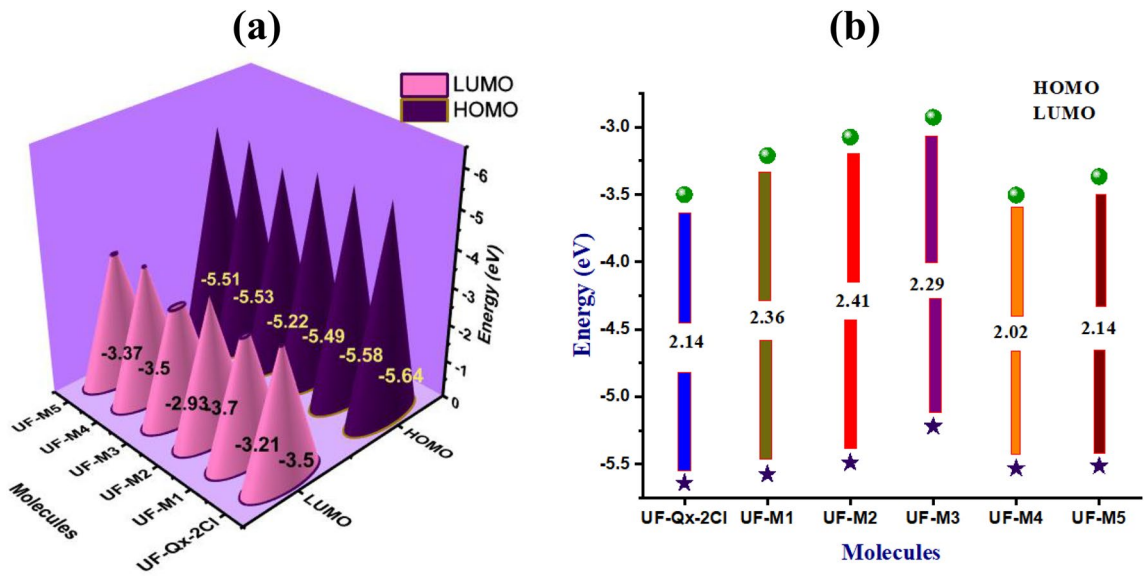

Fig. 5 Illustration of **a** HOMO–LUMO whereas **b** calculated E_g (band gap) of UF-Qx-2Cl and UF-M1–UF-M5

Table 2 Calculated values of HUMO, LUMO, bandgap (E_g), binding energy in gaseous state (E_b), binding energy in chloroform solvent (E_b), and reference's interaction coefficient (UF-Qx-2Cl) and designed moieties (UF-M1–UF-M5)

Molecule	HOMO (eV)	LUMO (eV)	E_g (eV)	E_b (eV) gaseous	E_b (eV) solvent	Interaction coefficient
UF-Qx-2Cl	−5.64	−3.50	2.14	0.36	0.49	0.69
UF-M1	−5.57	−3.21	2.36	0.35	0.46	0.69
UF-M2	−5.48	−3.07	2.41	0.39	0.47	0.69
UF-M3	−5.22	−2.92	2.29	0.38	0.48	0.69
UF-M4	−5.53	−3.50	2.02	0.32	0.45	0.69
UF-M5	−5.51	−3.36	2.14	0.35	0.47	0.69

moieties have negative charge density because of their electron-withdrawing ability and have reactive sites. Likewise, nitrogen in dicyanide has a denser negative region that acts as an active site at the terminal of the molecule where no such group or atom is present to cancel out their effect.

3.3 Quantum Chemical Descriptor Parameters

To check the kinetic stability of designed molecules and their chemical reactivity, different chemical parameters are used as chemical potential, hardness, softness, electronegativity, nucleophilicity, and total charge transfer. The calculated values of these parameters are given in Table 3.

Chemical potential is calculated by using the equation $\mu = (E_{HOMO} + E_{LUMO})/2$ [56] predicts the ability of the electronic cloud to escape [57]. Calculated values of chemical potential are highly negative indicating the designed molecules are highly reactive as well as highly stable too. Chemical hardness (η) and softness (S) of designed molecules UF-M4 and UF-M5 are better than reference molecules, indicating better reactivity along with the lowest bandgap.

Among these chemical parameters, electrophilicity (ω) and electronegativity (χ) parameters are used to predict the nature of the molecule towards accepting the electron. These factors are calculated by using Eqs. 5 and 6.

$$\text{Electronegetivity} = -\left(E_{HOMO} + E_{LUMO}\right)/2 \quad (5)$$

$$\text{Electrophilicity} = \chi^2/2\eta \quad (6)$$

UF-M4 and UF-M5 represented a better tendency toward accepting electrons as they have substituted with better electron-withdrawing groups. While remaining designed molecules also show values of (ω) and (χ) nearest to reference molecules. Total charge transfer (ΔN_{max}) is another parameter that is used to check the charge transfer rate in designed moieties. Same as other parameters, UF-M4 and UF-M5 figure out the better charge transfer in comparison to the reference molecule parameter that is used to check the charge transfer rate in designed moieties. Same as other parameters, UF-M4 and UF-M5 figure out the better charge transfer in comparison to the referencemolecule.

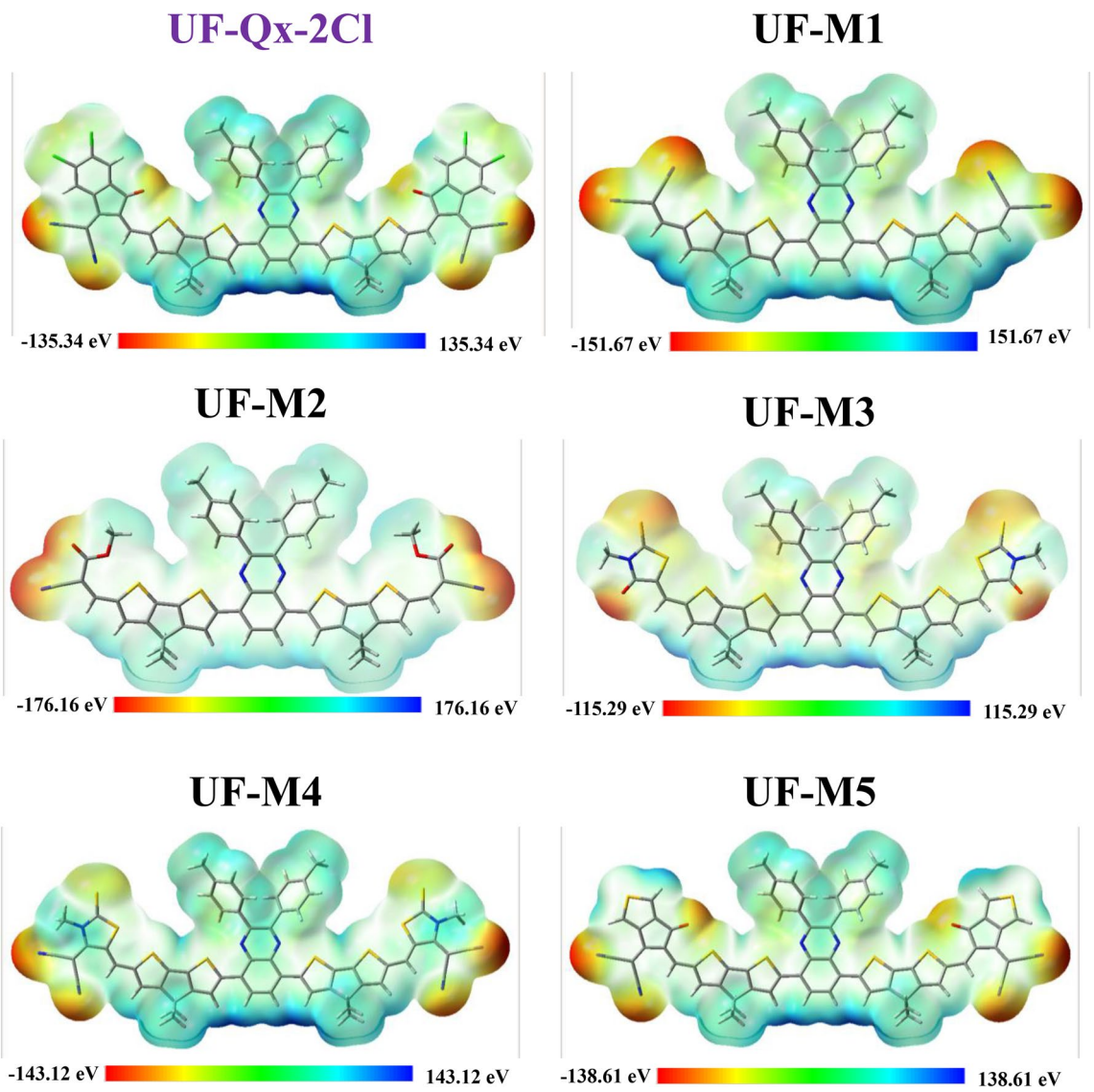

Fig. 6 MEP representation of reference and designed molecules

Table 3 Calculated values of quantum chemical descriptor parameters; chemical potential, hardness, softness, electronegativity, electrophilicity, and total charge transfer (ΔNmax)

Molecule	Chemical potential (μ)	Chemical hardness (η)	Chemical softness (S)	Electronegativity (χ)	Electrophilicity index (ω)	(ΔNmax)
UF-Qx-2Cl	−4.57	1.07	0.93	4.57	9.76	4.27
UF-M1	−4.39	1.18	0.85	4.39	8.16	3.72
UF-M2	−4.28	1.21	0.83	4.28	7.58	3.54
UF-M3	−4.07	1.15	0.87	4.07	7.24	3.55
UF-M4	−4.52	1.01	0.99	4.52	10.06	4.45
UF-M5	−4.44	1.07	0.93	4.44	9.18	4.13

3.4 UV–Vis Analysis and Spectral Representation

Absorption of light and its harvesting are the basic parameters of photovoltaics so it's necessary to study the UV–Vis absorption range of designed molecules. UV–Vis spectra provide insights into the electronic transition between HOMO & LUMO and charge transfer rate [13, 58, 59]. Absorption properties of R and UF-M1–UF-M5 molecules

are studied via selected level (mPW1PW91/6-31G(d,p)) through which reference molecule provided λ_{max} value nearest the gaseous state and chloroform as solvent phase mentioned in experimental data.

To manifest the precised absorption properties, we computed λ_{max} at 10 states in both, gaseous phase and chloroform, and the results are summarized in Tables 4 and 5. Calculated λ_{max} and experimental λ_{max} in both, gaseous phase and chloroform, oscillations strength (f_o), 1st transition energy (ΔE), concerning transition ($S_0 \rightarrow S_1$), and their configuration factor % are given in Tables 4 and 5.

Usually, 1st excitation state is considered among all of the 10 states because electron transition between HOMO and LUMO occurs in 1st excitation state along with high oscillation strength (f_o). The computed λ_{max} of the UF-Qx-2Cl in the solvent phase is 753 nm while an experimentally reported value of λ_{max} is 772 nm. When we studied the UF-M1–UF-M5 moieites in the gaseous phase, the observed values of λ_{max} are 617, 612, 650, 726, and 692 nm respectively for UF-M1–UF-M5 (Fig. 7a). But when we studied the same UF-M1–UF-M5 structures in the chloroform, they showed a redshift due to stable delocalized electrons by solvent, and observed values of λ_{max} for UF-M1–UF-M5 are 654, 637, 685, 789, and 742 nm respectively (Fig. 7b). Decreasing order trend of λ_{max} in the solvent phase is UF-M4 > UF-M5 > UF-M3 > UF-M2 > UF-M1.

Table 4 Calculated λ_{max} in gaseous phase along with oscillation factor and their concerned transitions

Molecule	Calculated λ_{max} (nm)	Experimental λ_{max} (nm)	Molecular states (n)	Electronic Transition	ΔE (eV)	f_o	Concerned Transitions	% Configuration Interaction	LHE
UF-Qx-2Cl	699	772	10	$S_0 \rightarrow S_1$	1.77	3.07	HOMO → LUMO	69	0.9991
UF-M1	617	–	10	$S_0 \rightarrow S_1$	2.01	2.10	HOMO → LUMO	70	0.9921
UF-M2	612	–	10	$S_0 \rightarrow S_1$	2.02	1.20	HOMO → LUMO	70	0.9369
UF-M3	650	–	10	$S_0 \rightarrow S_1$	1.91	2.23	HOMO → LUMO	70	0.9941
UF-M4	726	–	10	$S_0 \rightarrow S_1$	1.71	2.87	HOMO → LUMO	70	0.9987
UF-M5	692	–	10	$S_0 \rightarrow S_1$	1.79	3.02	HOMO → LUMO	70	0.9990

Table 5 Calculated λ_{max} (nm) of reference and designed moieties in solvent phase along with excitation energies and their concerned transitions

Molecule	Calculated λ_{max} (nm)	Experimental λ_{max} (nm)	Molecular states (n)	Electronic Transition	ΔE (eV)	f_o	Concerned Transitions	% Configuration Interaction	LHE
UF-Qx-2Cl	753	772	10	$S_0 \rightarrow S_1$	1.64	3.37	HOMO → LUMO	69	0.9996
UF-M1	654	–	10	$S_0 \rightarrow S_1$	1.90	2.47	HOMO → LUMO	70	0.9966
UF-M2	637	–	10	$S_0 \rightarrow S_1$	1.94	2.47	HOMO → LUMO	70	0.9966
UF-M3	685	–	10	$S_0 \rightarrow S_1$	1.81	2.61	HOMO → LUMO	69	0.9975
UF-M4	789	–	10	$S_0 \rightarrow S_1$	1.57	3.21	HOMO → LUMO	69	0.9994
UF-M5	742	–	10	$S_0 \rightarrow S_1$	1.67	3.39	HOMO → LUMO	69	0.9996

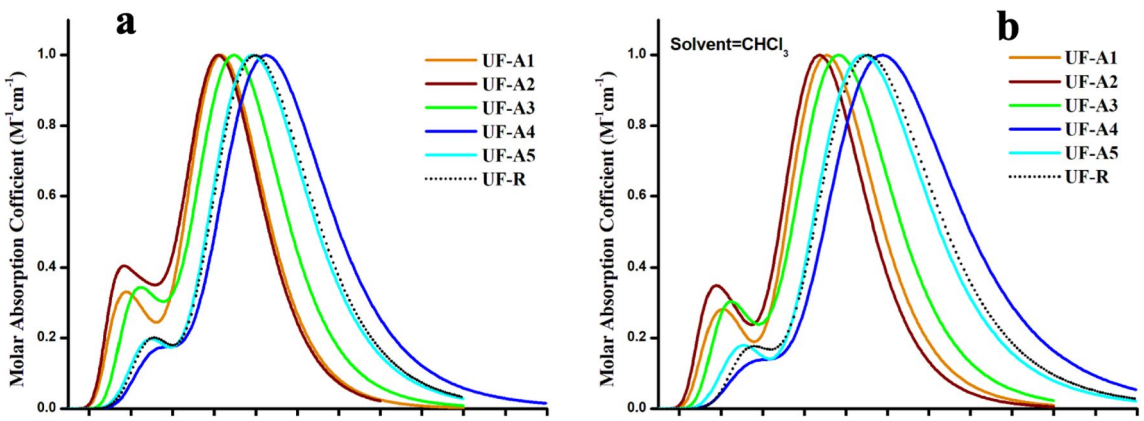

Fig. 7 Absorption spectra of UF-R and designed structures in **a** gaseous phase & **b** chloroform (solvent phase)

Among all of these, UF-M4 displayed the highest value of λ_{max} because of the cyano group, a strong electron moiety associated with electron pulling moieties that facilitate the electron transfer between donor and acceptor and lead to a shorter bandgap.

Another factor used to check the efficiency of the solar cell is light-harvesting efficiency (LHE) which can be computed via formula i.e., LHE = 1–10^{-fo} where f_o is the oscillation strength. Photocurrent response is directly proportional to LHE as, the higher the LHe, higher will be the response.

LHE values for designed molecules in both phases(gaseous and chloroform) are summarized in Tables 4 and 5. LHE value of all designed molecules is 0.99 in the solvent phase which means that all of these structures can be an auspicious candidate for photovoltaics in the future.

3.5 Dipole Moment

Another factor to estimate the efficiency of designed strucutres for efficient organic photovoltaics is the dipole-moment. The dipole moment depends on solubility of the molecules in a polar solvent i.e.,more polar groups: higher dipole moment. Besides polar groups, smoothness and flexibility of structure also relate to dipole moment, as molecules with high crystallinity have a low probability of charge transfer.

The smoothness of devised moieties leads to a higher rate of charge transfer which is a basic requirement of organic photovoltaics. Table 6 reveals the calculated dipole moment values of reference and UF-M1–UF-M5 in both phases. We studied in chloroform solvent phase, the value of dipole moment ranged from 2.53 to 15.47 D. Dipole moment usually acts in the direction of vector quantity while vector pointed from positive to negative in both cases, net dipole (molecular dipole) or individual dipole (between bonds). We also observed the vector and magnitude of dipole moment (Figure S1). UF-Qx-2Cl and UF-M1–UF-M4 showed the dipole moment in downward direction while UF-M5 showed in upward direction. Decreasing value trend of dipole moment in the solvent phase is UF-M1 > UF-M3 > UF-M2 > UF-M4 > UF-M5 > UF-Qx-2Cl. UF-M1 exhibited the 15.47 D value which is because of the 2-methylene malononitrile which acts as a strong electron-withdrawing group. While UF-M5 in designed moieties showed the lowest dipole moment value i.e., 2.92 D because of its lower solubility level in chloroform but still higher than the UF-Qx-2Cl which is approximately 2.53 D.

Table 6 Calculated values of dipole moment in both gaseous (μg) and solvent phase (μe) for UF-Qx-2Cl and devised structures UF-M1–UF-M5

Molecules	μg (Debye)	μe (Debye)	Δμ (Debye)
UF-Qx-2Cl	0.49	2.53	−2.04
UF-M1	10.30	15.47	−5.17
UF-M2	2.87	5.65	−2.79
UF-M3	7.14	11.67	−4.53
UF-M4	1.99	5.33	−3.33
UF-M5	3.60	2.92	0.68

3.6 TDM Analysis & E_b (Binding Energies)

Besides MEP, another important factor to compute the charge distribution between donor and acceptor is binding energy of the electron–hole pair (exciton). The energy required to produce the exciton is known as the binding energy (E_b). We calculated binding energies of the reference molecule and designed moieties by using Eq. 8.

$$E_b = E_g - E_x \tag{8}$$

where E_g is HOMO and LUMO energies difference while E_x is the excitation energy. Exciton generation depends on binding energies, the lower the binding energies: the higher will be exciton generation rate and results in higher J_{sc} (current charge density). Calculated values of binding energies for UF-Qx-2Cl and UF-M1–UF-M5, under both conditions of gaseous and solvent phases are provided in Table 2. Trend order of E_b for UF-Qx-2Cl and UF-M1–UF-M5 in solvent phase is UF-M4 < UF-M1 < UF-M2 = UF-M5 < UF-M3 < UF-Qx-2Cl. UF-M4 exhibited the least E_b among all the designed moieties while all other understudy moieties also exhibited an E_b value smaller than reference, which can be used for effectual charge transfer in the proficient organic solar cells.

Besides binding energies, TDM analysis also helps to test and clarify the quantum geometry of molecules by their excitation measures. It explicates the exciton generation and charge density movement from electron-donating to electron-withdrawing moiety via conjugated π electrons [60]. In TDM, hydrogens atoms are excluded because of their negligible contributions while the remaining atoms are distributed in 3 components (C = core, D = donor, and A = acceptor) in our designed molecules and UF-Qx-2Cl Fig. 8.

The bottom and left sides of the TDM graph showed the number of atoms contributing to charge distribution between donor and acceptor while the right side y-axis showed the charge density of contributing atoms.

Uniform distribution of charge between donor and acceptor subunits in UF-Qx-2Cl and UF-M1–UF-M5 (designed structures) exhibited favorable diagonal and off-diagonal attribution. The charge on the donor portion of UF-M4 is more consistent, and it betray excellent diagonal and off-diagonal charge transfer across donor–acceptor, demonstrating that this newly designed moiety has less

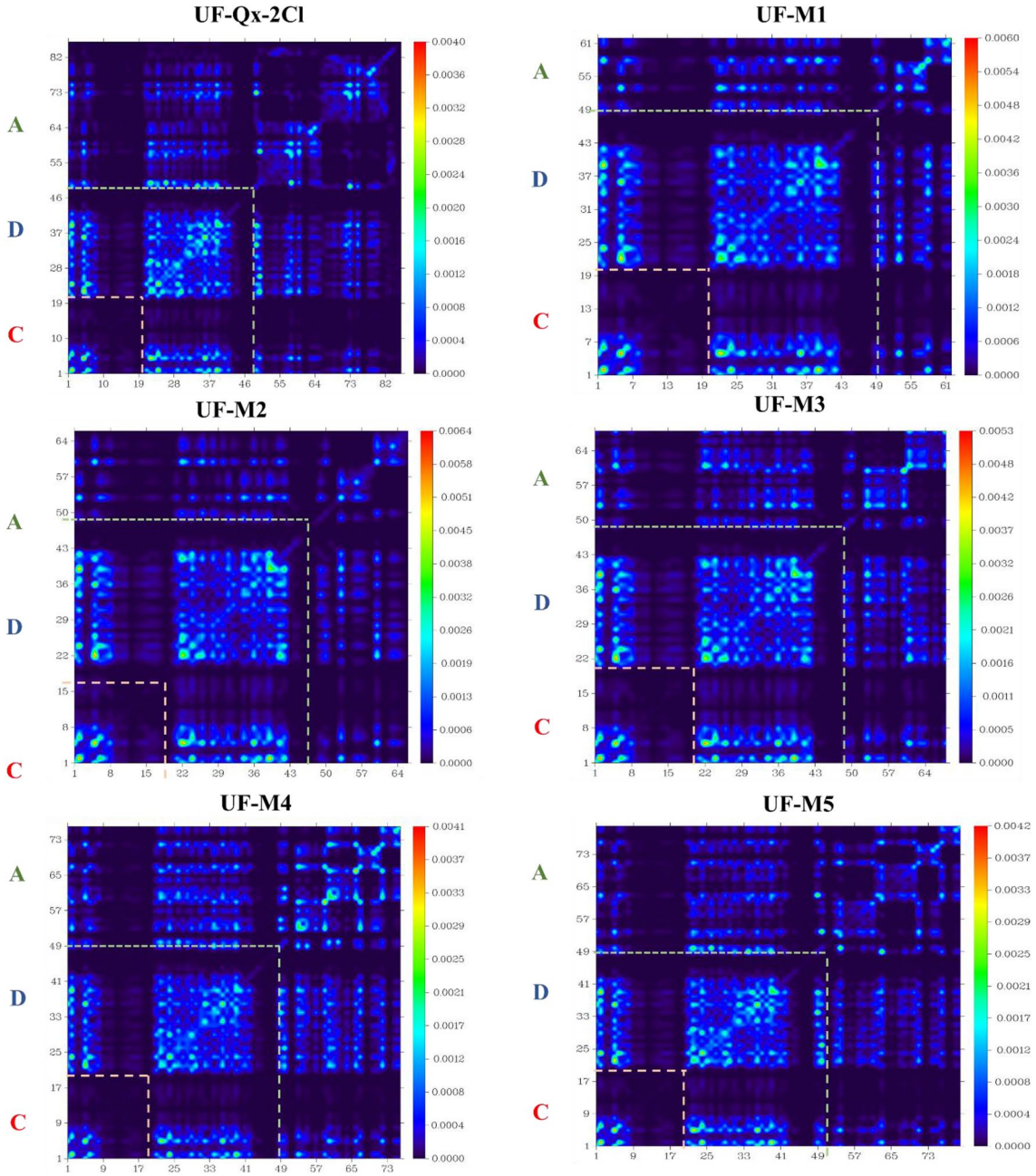

Fig. 8 TDM plot of UF-Qx-2Cl (R) and designed structures (UF-M1–UF-M5) where C = core, D = donor, and A = Acceptor

electron coupling, as shown by simpler exciton dissociation, which is required for constructing effective OSCs. Charge distribution and interaction coefficient order of UF-Qx-2Cl and UF-M1–UM-M5 is UF-M4 < UF-M1 < UF-M2 = UF-M5 < UF-M3 < UF-Qx-2Cl (Table 2). According to decreasing trend of dissociation coefficient, UF-M4 exhibits the enhanced charge transfer from donor subunit to acceptor because of the π–π* stream and conjugated system.

3.7 DOS Analysis (Density of State)

The density of states is a population of many energy levels that can be used for excitation, or charge generation. DOS analysis is used to view the contribution of the various components in the charge distribution between HOMO and LUMO in the designated moieties. Mulliken charge distribution has been used to ensure FMO findings. DOS analysis also predicts the value of HOMO and LUMO. DOS calculations have been performed through Gaussian software by

using a selected method and basis set, while the spectra are designed by using PyMolyze 1.1 software and are represented in Fig. 9. The core, donor, and acceptor components of a DOS spectral representation for reference and designed moieties are represented via blue, green, and red colors, respectively, while black color represented the overall charge

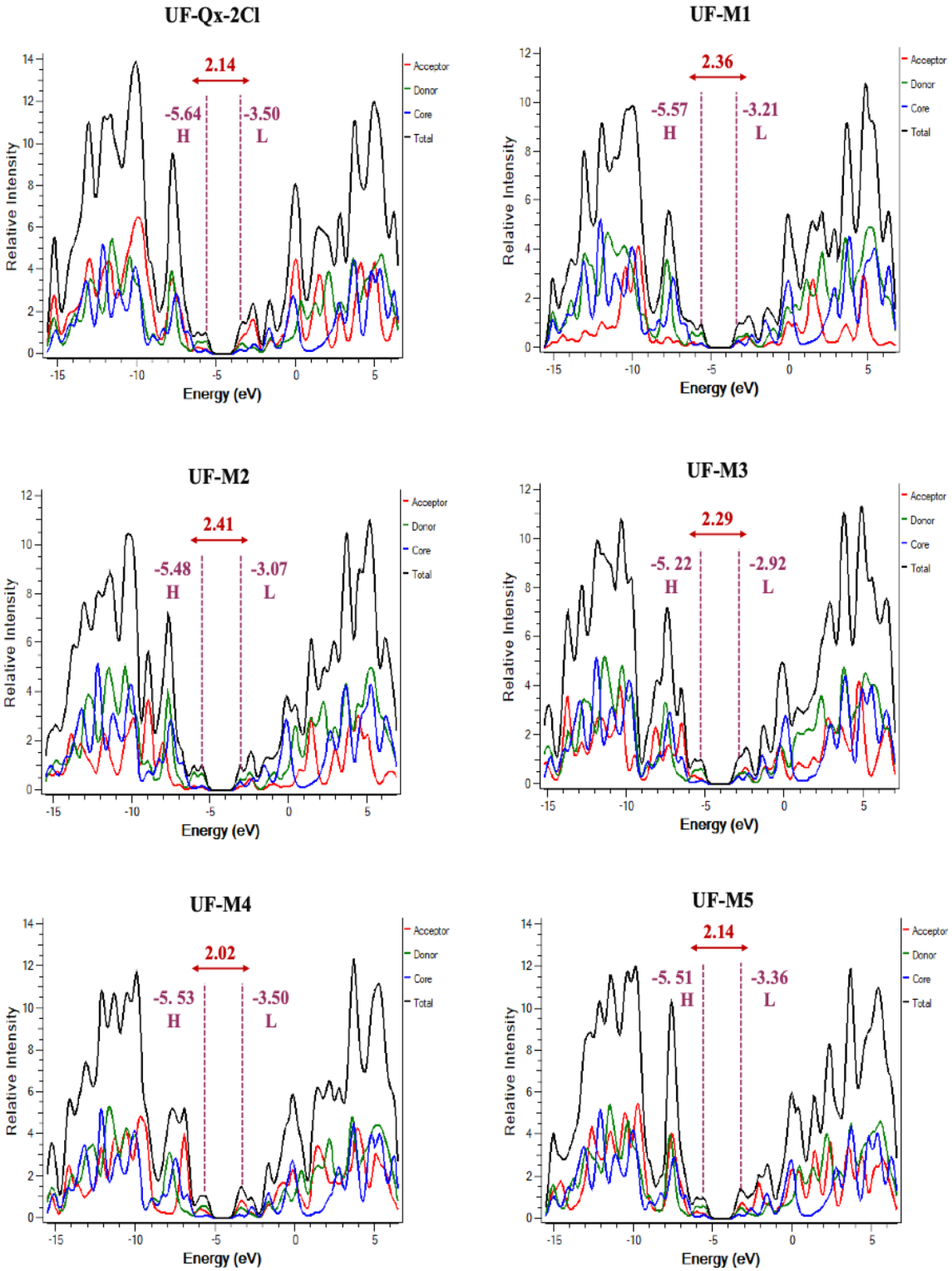

Fig. 9 Graphical representation of density of state analysis (DOS) for reference and designed structures

Table 7 Orbital contribution of Core, Donor, and Acceptor subunits of UF-Qx-2Cl and designed structures

Molecules		Acceptor	Core	Donor
UF-Qx-2Cl	HOMO	23.0	59.5	17.5
	LUMO	45.1	36.8	18.1
UF-M1	HOMO	16.5	64.0	19.5
	LUMO	24.6	44.9	30.5
UF-M2	HOMO	11.3	70.4	18.3
	LUMO	15.8	45.4	38.8
UF-M3	HOMO	21.2	62.3	16.5
	LUMO	28.0	39.5	32.5
UF-M4	HOMO	28.3	56.4	15.3
	LUMO	48.3	35.0	16.6
UF-M5	HOMO	23.3	59.7	17.0
	LUMO	42.6	37.5	20.0

distribution on the structure. Orbital contribution of the acceptor, core and donor of reference and designed moieties in HOMO–LUMO raising are given in Table 7. Computed results of bandgap through FMO and DOS are the same according to quantitative orbital contribution values (Table 7), the acceptor subunit of UF-M4 exhibited better contribution in raising HOMO and LUMO values. UF-M5 showed a similar contribution to reference in raising HOMO and LUMO values while other designed moieties' results are also comparable to these moieties. The core subunit also contributed to raising the HOMO–LUMO values for better charge transfer from donor to acceptor.

3.8 Reorganization Energy

By excitation process, excitons generate and then splits into electrons and holes. After generation, these electrons and holes move towards their particular electrodes and are generally known as charge transfer. Charge transfer is a basic parameter of organic photovoltaics which get influenced by the geometry and flexibility of the structure. Charge transfer is usually calculated by electron (λ_e) and hole (λ_h) mobility energies (reorganization energies) via Eqs. 2 and 3. Charge transfer and reorganization energies have inverse relations i.e., lower the reorganization energy: higher the charge transfer. Reorganization energies are of two types, intrinsic and extrinsic, among them we considered here are intrinsic energies based on internal geometrical alterations while extrinsic based on surroundings (solvent chloroform) effect. Calculated values of electron and hole reorganization energies (λ_e and λ_h) are provided in Table 8.

According to Table 8, UF-Qx-2Cl represented the 0.00818 eV for λ_e which is smaller than all designed molecules. λ_e increasing order for designed structures is UF-M5 < UF-M1 < UF-M4 < UF-M3 < UF-M2 as their respective values are 0.00846 < 0.00936 < 0.00990 < 0.01000 < 0.01063. Although the λ_e value of UF-M5 is comparable to reference but still higher which indicates that our designed moieties act as acceptor molecules which get confirmed through λ_h values of designed moieties. λ_h increasing trend is UF-M4 < UF-M5 < UF-Qx-2Cl < UF-M2 < UF-M3 < UF-M1 as their respective values are 0.00766, 0.00827, 0.00850, 0.00877, 0.00902, and 0.23283.

Table 8 Electron and hole mobility energies (λ_e and λ_h) for UF-Qx-2Cl and UF-M1–UF-M5 designed series

Molecules	λ_- (eV)	λ_+ (eV)
UF-Qx-2Cl	0.00818	0.00850
UF-M1	0.00936	0.23283
UF-M2	0.01063	0.00877
UF-M3	0.01000	0.00902
UF-M4	0.00990	0.00766
UF-M5	0.00846	0.00827

According to Table 8, UF-M4, and UF-M5 have better hole mobility than a reference by the significant difference in λ_h values. λ_h values of UF-M2 and UF- M3 is comparable to reference molecule while UF-M1 represented too much higher value.

3.9 Open-Circuit Voltage (Voc)

The open-circuit voltage, or V_{OC}, is the greatest voltage a solar cell can produce while the current is zero [61]. The total efficiency of OSCs may be determined using V_{oc}. It is proportional to the energy of the donor material's HOMO and the acceptor material's LUMO that has been provided to the external circuit. Intermolecular interactions and compact packing of molecules can reduce the energy-gap. As a result, the Voc tends to drop as the energy gap closes. It aids in demonstrating the highest amount of current that an organic solar cell can produce. The open-circuit voltage is directly affected by several things, light intensity, charge recombination, light source, charge collecting at electrodes, and varying amounts of energy are among them. V_{oc} is calculated by using Eq. 9.

$$V_{OC} = \frac{E_{LUMOofacceptor} - E_{HOMOofdonor}}{e} - 0.3 \quad (9)$$

In Eq. 9, e is the charge on the molecular framework, which we set to 1 for computations, and 0.3 is the charge production offset at the molecular interface. PBDB-T [62], a highly efficient donor with HOMO and LUMO values of − 4.93 eV and − 2.27 eV was chosen with our designed structures to generate the interface of donor–acceptor and graphically represented in Fig. 10.

V_{oc} value of designed molecules represented the following trend, UF-M3 > UF-M2 > UF-M1 > UF-M5 > UF-M4

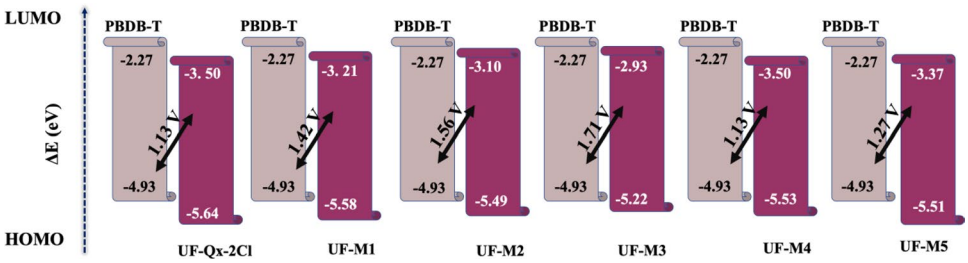

Fig. 10 Open-circuit voltage (V_{oc}) diagram of all moieties (R & designed moieties) as acceptor with PDBD-T (ΔE)

as their respective V_{oc} values are 1.71 > 1.56 > 1.42 > 1.27 > 1.13 V whereas V_{oc} value for UF-QX-2Cl/PDBD-T interface is 1.13 V. Additionally, we evaluated the V_{oc} of designed moieties with large band gap polymeric donor material P3HT, as HOMO and LUMO values for P3HT are − 5.12 eV and − 2.84 eV respectively. Observed trend of V_{oc} for reference and designed moities is as UF-M3 > UF-M2 > UF-M1 > UF-M5 > UF-M4 ≈ UF-Qx-2Cl with their respective values as 1.91 > 1.76 > 1.62 > 1.47 > 1.33 ≈ 1.33 V (Figure S2). The V_{oc} values of developed molecules are higher than the reference except UF-M4 moleculed whose value is comparable to reference molecule.

4 Conclusion

The widespread availability and low installation costs of solar energy have increased its contribution in recent years. To take advantage of these benefits, the current study relies on designing A-D-A-D-A type acceptor contributors for OSCs by offering a variety of encouraging acceptors as terminal units. We computationally designed five molecules (UF-M1–UF-M5) by substitution of acceptor moieties in the reference molecule (UF-Qx-2Cl). These designed molecules were optimized at mPW1PW91/6-31G (d,p) level, as by this method, the reference molecule predicted values were nearest to experimental data. Calculated HOMO–LUMO values, their bandgap, and further their energies (λ_{max})in both gaseous and solvent phases. Band-gap of designed models falls in between the 2.03–2.42 eV range, as UF-M4 shows a lower band-gap than reference while all others have comparable to UF-Qx-2Cl. The dipole moment of all designed structures is higher than the reference molecule means having a higher charge transfer rate in the solvent phase, DOS analysis also confirmed that UF-M4 and UF-M5 have better properties than reference which is confirmed by the table of quantitative contributions of subunits. Further, the TDM analysis was performed to confirm the results and modelized structures represented the higher charge dissociation between donor–acceptor and higher J_{sc}. Chemical quantum parameters results are also comparable to reference. UF-M4 and UF-M5 showed better hole and electron mobility competency to reference. We calculated the V_{oc} of designed molecules and the results are comparable to our reference molecule. Overall molecules, UF-M4 showed better results among all designed models which get confirmed through different computational confirmatory analyses while the remaining designed structures are also comparable to reference as they show some parameters better than reference. As a result, newly intended structures UF-M4 can increase the device's working aptness and might be utilized as major donor materials in the construction of future adept OSCs.

Supplementary Information The online version contains supplementary material available at https://doi.org/10.1007/s13391-022-00378-0.

Acknowledgements The authors acknowledge the Department of Chemistry and thank Punjab Bio-energy Institute (PBI) for financial and technical support, University of Agriculture (UAF), Faisalabad 38000, Pakistan. The authors would like to thank the Deanship of Scientific Research at Umm Al-Qura. University for supporting this work by Grant Code: (22UQU4331174DSR26).

Declarations

Conflict of interest The authors declare no competing financial interest.

References

1. Kumaresan, P., Vegiraju, S., Ezhumalai, Y., Yau, S.L., Kim, C., Lee, W.-H., Chen, M.-C.: Fused-thiophene based materials for organic photovoltaics and dye-sensitized solar cells. Polymers **6**, 2645–2669 (2014)
2. Pao, H.-T., Li, Y.-Y., Fu, H.-C.: Clean energy, non-clean energy, and economic growth in the MIST countries. Energy Policy **67**, 932–942 (2014)
3. Twidell, J., Weir, T.: Renewable Energy Resources. Routledge, London (2015)
4. Singh, N., Nyuur, R., Richmond, B.: Renewable energy development as a driver of economic growth: evidence from multivariate panel data analysis. Sustainability **11**, 2418 (2019)
5. Wright, R., Shin, H., Trentmann, F.: From World Power Conference to World Energy Council, World Energy Council (2013)
6. Chen, Y., Wan, X., Long, G.: High performance photovoltaic applications using solution-processed small molecules. Acc. Chem. Res. **46**, 2645–2655 (2013)
7. Ans, M., Iqbal, J., Eliasson, B., Ayub, K.: Opto-electronic properties of non-fullerene fused-undecacyclic electron acceptors for organic solar cells. Comput. Mater. Sci. **159**, 150–159 (2019)
8. Hagfeldt, A., Boschloo, G., Sun, L., Kloo, L., Pettersson, H.: Dye-sensitized solar cells. Chem. Rev. **110**, 6595–6663 (2010)

9. Mishra, A., Bäuerle, P.: Small molecule organic semiconductors on the move: promises for future solar energy technology. Angew. Chem. Int. Ed. **51**, 2020–2067 (2012)
10. Afzaal, M., O'Brien, P.: Recent developments in II–VI and III–VI semiconductors and their applications in solar cells. J. Mater. Chem. **16**, 1597–1602 (2006)
11. Yuan, J., Zhang, Y., Zhou, L., Zhang, G., Yip, H.-L., Lau, T.-K., Lu, X., Zhu, C., Peng, H., Johnson, P.A.: Single-junction organic solar cell with over 15% efficiency using fused-ring acceptor with electron-deficient core. Joule **3**, 1140–1151 (2019)
12. Sun, D., Meng, D., Cai, Y., Fan, B., Li, Y., Jiang, W., Huo, L., Sun, Y., Wang, Z.: Non-fullerene-acceptor-based bulk-heterojunction organic solar cells with efficiency over 7%. J. Am. Chem. Soc. **137**, 11156–11162 (2015)
13. Ahmed, S., Kalita, D.J.: End-capped group manipulation of non-fullerene acceptors for efficient organic photovoltaic solar cells: a DFT study. Phys. Chem. Chem. Phys. **22**, 23586–23596 (2020)
14. Ala'a, F.E., Sun, J.-P., Hill, I.G., Welch, G.C.: Recent advances of non-fullerene, small molecular acceptors for solution processed bulk heterojunction solar cells. J. Mater. Chem. A **2**, 1201–1213 (2014)
15. Li, H., Hwang, Y.J., Courtright, B.A., Eberle, F.N., Subramaniyan, S., Jenekhe, S.A.: Fine-Tuning the 3D structure of nonfullerene electron acceptors toward high-performance polymer solar cells. Adv. Mater. **27**, 3266–3272 (2015)
16. Zhong, Y., Trinh, M.T., Chen, R., Wang, W., Khlyabich, P.P., Kumar, B., Xu, Q., Nam, C.-Y., Sfeir, M.Y., Black, C.: Efficient organic solar cells with helical perylene diimide electron acceptors. J. Am. Chem. Soc. **136**, 15215–15221 (2014)
17. Zhao, W., Li, S., Yao, H., Zhang, S., Zhang, Y., Yang, B., Hou, J.: Molecular optimization enables over 13% efficiency in organic solar cells. J. Am. Chem. Soc. **139**, 7148–7151 (2017)
18. Meng, D., Sun, D., Zhong, C., Liu, T., Fan, B., Huo, L., Li, Y., Jiang, W., Choi, H., Kim, T.: High-performance solution-processed non-fullerene organic solar cells based on selenophene-containing perylene bisimide acceptor. J. Am. Chem. Soc. **138**, 375–380 (2016)
19. Hwang, Y.J., Li, H., Courtright, B.A., Subramaniyan, S., Jenekhe, S.A.: Nonfullerene polymer solar cells with 8.5% efficiency enabled by a new highly twisted electron acceptor dimer. Adv. Mater. **28**, 124–131 (2016)
20. Kan, B., Feng, H., Wan, X., Liu, F., Ke, X., Wang, Y., Wang, Y., Zhang, H., Li, C., Hou, J.: Small-molecule acceptor based on the heptacyclic benzodi (cyclopentadithiophene) unit for highly efficient nonfullerene organic solar cells. J. Am. Chem. Soc. **139**, 4929–4934 (2017)
21. Ma, Y., Zhang, M., Wan, S., Yin, P., Wang, P., Cai, D., Liu, F., Zheng, Q.: Efficient organic solar cells from molecular orientation control of m-series acceptors. Joule **5**, 197–209 (2021)
22. Li, Y., Zhong, L., Gautam, B., Bin, H.-J., Lin, J.-D., Wu, F.-P., Zhang, Z., Jiang, Z.-Q., Zhang, Z.-G., Gundogdu, K.: A near-infrared non-fullerene electron acceptor for high performance polymer solar cells. Energy Environ. Sci. **10**, 1610–1620 (2017)
23. Shi, X., Zuo, L., Jo, S.B., Gao, K., Lin, F., Liu, F., Jen, A.K.-Y.: Design of a highly crystalline low-band gap fused-ring electron acceptor for high-efficiency solar cells with low energy loss. Chem. Mater. **29**, 8369–8376 (2017)
24. Gao, H.H., Sun, Y., Wan, X., Ke, X., Feng, H., Kan, B., Wang, Y., Zhang, Y., Li, C., Chen, Y.: A new nonfullerene acceptor with near infrared absorption for high performance ternary-blend organic solar cells with efficiency over 13%. Adv. Sci. **5**, 1800307 (2018)
25. Huang, C., Liao, X., Gao, K., Zuo, L., Lin, F., Shi, X., Li, C.-Z., Liu, H., Li, X., Liu, F.: Highly efficient organic solar cells based on S, N-heteroacene non-fullerene acceptors. Chem. Mater. **30**, 5429–5434 (2018)
26. Lin, Y., Wang, J., Zhang, Z.G., Bai, H., Li, Y., Zhu, D., Zhan, X.: An electron acceptor challenging fullerenes for efficient polymer solar cells. Adv. Mater. **27**, 1170–1174 (2015)
27. Yang, W., Wang, W., Wang, Y., Sun, R., Guo, J., Li, H., Shi, M., Guo, J., Wu, Y., Wang, T.: Balancing the efficiency, stability, and cost potential for organic solar cells via a new figure of merit. Joule **5**, 1209–1230 (2021)
28. Yu, Z.-P., Liu, Z.-X., Chen, F.-X., Qin, R., Lau, T.-K., Yin, J.-L., Kong, X., Lu, X., Shi, M., Li, C.-Z.: Simple non-fused electron acceptors for efficient and stable organic solar cells. Nat. Commun. **10**, 1–9 (2019)
29. Wen, T.J., Liu, Z.X., Chen, Z., Zhou, J., Shen, Z., Xiao, Y., Chen, H.: Simple non-fused electron acceptors leading to efficient organic photovoltaics. Angew. Chem. Int. Ed. **60**(23), 12964–12970 (2021)
30. Chen, Y.N., Li, M., Wang, Y., Wang, J., Zhang, M., Zhou, Y., Yang, J., Liu, Y., Liu, F., Tang, Z.: A fully non-fused ring acceptor with planar backbone and near-IR absorption for high performance polymer solar cells. Angew. Chem. Int. Ed. **59**, 22714–22720 (2020)
31. Pang, S., Zhou, X., Zhang, S., Tang, H., Dhakal, S., Gu, X., Duan, C., Huang, F., Cao, Y.: Nonfused nonfullerene acceptors with an A-D–A′–D–A framework and a Benzothiadiazole core for high-performance organic solar cells. ACS Appl. Mater. Interfaces **12**, 16531–16540 (2020)
32. Li, S., Zhan, L., Lau, T.K., Yu, Z.P., Yang, W., Andersen, T.R., Fu, Z., Li, C.Z., Lu, X., Shi, M.: Near-infrared nonfullerene acceptors based on benzobis (thiazole) unit for efficient organic solar cells with low energy loss. Small Methods **3**, 1900531 (2019)
33. Cao, J., Qu, S., Yang, L., Wang, H., Du, F., Yu, J., Tang, W.: Asymmetric simple unfused acceptor enabling over 12% efficiency organic solar cells. Chem. Eng. J. **412**, 128770 (2021)
34. Lee, J., Ko, S.J., Seifrid, M., Lee, H., Luginbuhl, B.R., Karki, A., Ford, M., Rosenthal, K., Cho, K., Nguyen, T.Q.: Bandgap narrowing in non-fullerene acceptors: single atom substitution leads to high optoelectronic response beyond 1000 nm. Adv. Energy Mater. **8**, 1801212 (2018)
35. Lu, B.-S., Zhang, Y., Hu, T.-Y., Ma, Y.-F., Zhu, Y.-N., Liu, D.-W., Zhang, Z.-Q., Wang, E., Ma, W., Zhang, H.-L.: Non-fullerene acceptors based on multiple non-covalent interactions for low cost and air stable organic solar cells. Org. Electron. **93**, 106132 (2021)
36. Sui, D., Wu, M., Liu, Y., Yang, Y., Zhang, H., Ma, Y., Zhang, L., Chen, Y.: High performance Li-ion capacitor fabricated with dual graphene-based materials. Nanotechnology **32**, 015403 (2020)
37. Chang, M., Zhang, Y., Lu, B.-S., Sui, D., Wang, F., Wang, J., Yang, Y., Kan, B.: The design of quinoxaline based unfused non-fullerene acceptors for high performance and stable organic solar cells. Chem. Eng. J. **427**, 131473 (2022)
38. Pang, S., Liu, L., Sun, X., Dong, S., Wang, Z., Zhang, R., Guo, Y., Li, W., Zheng, N., Duan, C.: A wide-bandgap conjugated polymer based on quinoxalino [6, 5-f] quinoxaline for fullerene and non-fullerene polymer solar cells. Macromol. Rapid Commun. **40**, 1900120 (2019)
39. Yao, H., Ye, L., Zhang, H., Li, S., Zhang, S., Hou, J.: Molecular design of benzodithiophene-based organic photovoltaic materials. Chem. Rev. **116**, 7397–7457 (2016)
40. Sun, C., Pan, F., Bin, H., Zhang, J., Xue, L., Qiu, B., Wei, Z., Zhang, Z.-G., Li, Y.: A low cost and high performance polymer donor material for polymer solar cells. Nat. Commun. **9**, 1–10 (2018)
41. Iqbal, J., Ayub, K.: Enhanced electronic and non-linear optical properties of alkali metal (Li, Na, K) doped boron nitride nanocages. J. Alloy Compd. **687**, 976–983 (2016)
42. Frisch, M., Trucks, G., Schlegel, H.B., Scuseria, G.E., Robb, M.A., Cheeseman, J.R., Scalmani, G., Barone, V., Mennucci, B.,

Petersson, G.: gaussian 09, Revision d. 01, Gaussian, Inc., Wallingford CT, 201 (2009).
43. Civalleri, B., Zicovich-Wilson, C.M., Valenzano, L., Ugliengo, P.: B3LYP augmented with an empirical dispersion term (B3LYP-D*) as applied to molecular crystals. CrystEngComm **10**, 405–410 (2008)
44. Yanai, T., Tew, D.P., Handy, N.C.: A new hybrid exchange–correlation functional using the Coulomb-attenuating method (CAM-B3LYP). Chem. Phys. Lett. **393**, 51–57 (2004)
45. Adamo, C., Barone, V.: Exchange functionals with improved long-range behavior and adiabatic connection methods without adjustable parameters: thew m PW and m PW1PW models. J. Chem. Phys. **108**, 664–675 (1998)
46. Chai, J.-D., Head-Gordon, M.: Long-range corrected hybrid density functionals with damped atom–atom dispersion corrections. Phys. Chem. Chem. Phys. **10**, 6615–6620 (2008)
47. Deschenes, L.A., David A.: Vanden BoutUniversity of Texas, Origin 6.0: Scientific Data Analysis and Graphing Software Origin Lab Corporation (formerly Microcal Software, Inc.). Web site: www.originlab.com. Commercial price: 595.Academicprice: 446, ACS Publications, (2000)
48. Lu, T., Chen, F.: Multiwfn: a multifunctional wavefunction analyzer. J. Comput. Chem. **33**, 580–592 (2012)
49. Tenderholt, A.L.: PyMOlyze: a program to analyze quantum chemistry calculations, version, (2019)
50. Ans, M., Manzoor, F., Ayub, K., Nawaz, F., Iqbal, J.: Designing dithienothiophene (DTT)-based donor materials with efficient photovoltaic parameters for organic solar cells. J. Mol. Model. **25**, 1–12 (2019)
51. Zhou, J., Wan, X., Liu, Y., Long, G., Wang, F., Li, Z., Zuo, Y., Li, C., Chen, Y.: A planar small molecule with dithienosilole core for high efficiency solution-processed organic photovoltaic cells. Chem. Mater. **23**, 4666–4668 (2011)
52. Ans, M., Iqbal, J., Ahmad, Z., Muhammad, S., Hussain, R., Eliasson, B., Ayub, K.: Designing Three-dimensional (3D) non-fullerene small molecule acceptors with efficient photovoltaic parameters. ChemistrySelect **3**, 12797–12804 (2018)
53. Ans, M., Ayub, A., Alwadai, N., Rasool, A., Zahid, M., Iqbal, J., Al-Buriahi, M.: Simultaneously enhanced efficiency of eco-friendly structural characterization of the dithienocyclopentacarbazole donor based acceptors with narrow bandgap for high-performance organic solar cells. J. Phys. D Appl. Phys. **55**, 235501 (2022)
54. Ans, M., Ayub, K., Bhatti, I.A., Iqbal, J.: Designing indacenodithiophene based non-fullerene acceptors with a donor–acceptor combined bridge for organic solar cells. RSC Adv. **9**, 3605–3617 (2019)
55. Ans, M., Ayub, K., Muhammad, S., Iqbal, J.: Development of fullerene free acceptors molecules for organic solar cells: a step way forward toward efficient organic solar cells. Comput. Theor. Chem. **1161**, 26–38 (2019)
56. Rad, A.S., Ayub, K.: Nonlinear optical and electronic properties of Cr-, Ni-, and Ti-substituted C20 fullerenes: a quantum-chemical study. Mater. Res. Bull. **97**, 399–404 (2018)
57. Musawwir, A., Farhat, A., Khera, R.A., Ayub, A.R., Iqbal, J.: Theoretical and computational study on electronic effect caused by electron withdrawing/electron-donating groups upon the coumarin thiourea derivatives. Comput. Theor. Chem. **1201**, 113271 (2021)
58. Hachi, M., Slimi, A., Fitri, A., ElKhattabi, S., Benjelloun, A.T., Benzakour, M., Mcharfi, M.: New small organic molecules based on thieno [2, 3-b] indole for efficient bulk heterojunction organic solar cells: a computational study. Mol. Phys. **118**, e1662956 (2020)
59. Ans, M., Paramasivam, M., Ayub, K., Ludwig, R., Zahid, M., Xiao, X., Iqbal, J.: Designing alkoxy-induced based high performance near infrared sensitive small molecule acceptors for organic solar cells. J. Mol. Liq. **305**, 112829 (2020)
60. Farhat, A., Khera, R.A., Iqbal, S., Iqbal, J.: Tuning the optoelectronic properties of Subphthalocyanine (SubPc) derivatives for photovoltaic applications. Opt. Mater. **107**, 110154 (2020)
61. Arshad, M.N., Shafiq, I., Khalid, M., Asiri, A.M.: Exploration of the intriguing photovoltaic behavior for fused indacenodithiophene-based A-D–A conjugated systems: a DFT model study. ACS Omega **7**, 11606–11617 (2022)
62. Zheng, Z., Yao, H., Ye, L., Xu, Y., Zhang, S., Hou, J.: PBDB-T and its derivatives: a family of polymer donors enables over 17% efficiency in organic photovoltaics. Mater. Today **35**, 115–130 (2020)

Publisher's Note Springer Nature remains neutral with regard to jurisdictional claims in published maps and institutional affiliations.

Springer Nature or its licensor (e.g. a society or other partner) holds exclusive rights to this article under a publishing agreement with the author(s) or other rightsholder(s); author self-archiving of the accepted manuscript version of this article is solely governed by the terms of such publishing agreement and applicable law.